

110 2 /
010300

NASA Technical Memorandum 107372

Local and Global Bifurcations of Flow Fields During Physical Vapor Transport: Application to a Microgravity Experiment

W.M.B. Duval
*Lewis Research Center
Cleveland, Ohio*

N.B. Singh
*Northrop Grumman Science & Technology Center
Pittsburgh, Pennsylvania*

M.E. Glicksman
*Rensselaer Polytechnic Institute
Troy, New York*

Prepared for the
Tenth American Conference on Crystal Growth
sponsored by the American Association for Crystal Growth
Vail, Colorado, August 4–9, 1996



National Aeronautics and
Space Administration

LOCAL AND GLOBAL BIFURCATIONS OF FLOW FIELDS DURING PHYSICAL VAPOR TRANSPORT: APPLICATION TO A MICROGRAVITY EXPERIMENT

W.M.B. Duval, NASA Lewis Research Center, Cleveland, Ohio 44135

N.B. Singh, Northrop Grumman Science & Technology Center, Pittsburg, PA 15235-5098

M.E. Glicksman, Rensselaer Polytechnic Institute, Troy, N.Y. 12180

1. Introduction

We investigate the local and global bifurcations of bulk fluid flow to determine its dynamical state. These flows occur during crystal growth of mercurous chloride by the physical vapor transport (PVT) process. The dynamical state of the flow field is analyzed for a parameter space which corresponds to ground based experimental conditions. In particular, two sets of experiments are considered which corresponds to: (a) Laser Doppler Velocimetry (LDV) measurements of the flow field by Kim et al. [1], and (b) Correlation of crystal quality with growth conditions of mercurous chloride, Singh et al. [2]. Crystal quality is correlated to the scattering patterns of light through the crystals. In view of these experiments, we analyze the physics of PVT inside a rectangular enclosure through a mathematical model to provide insight into various trends. A parametric setting is selected which will lead to a meaningful microgravity experiment.

PVT is advantageous for a material such as mercurous chloride due to its decomposition near its melting point [3], and its high vapor pressure at typical growth conditions ($T = 345^{\circ}C$, $P_A = 289$ torr). Various vapor transport processes and their convective characteristics are discussed by Rosenberger [4]. The wide infra-red transmission range (.36 to 20 μm) of mercurous chloride makes it attractive for applications in acousto-optic optoelectronic devices such as acousto-optic tunable filters, Bragg cells, and spectrum analyzers. PVT involves sublimation from a heated source material, transport through a rarified inert gas, and condensation to a lower temperature heat sink inside an enclosure. The dynamical state of the flow field during PVT is affected by the external conditions through the thermal settings, gaseous components, ampoule geometry, and orientation of the enclosure with respect to gravity.

There have been numerous works which investigate PVT under various conditions and ampoule geometry. Greenwell, Markham and Rosenberger [5] show that, even in the absence of gravity, non-uniform concentration gradients occur near the vapor crystal interface for cylindrical ampoules oriented horizontally. For vertically oriented cylinders, Markham Greenwell and Rosenberger [6] show that convection is stabilized for solutally/thermally dominated flow when transport is against/assisted by gravity; otherwise convective cells occur in both systems beyond a certain parametric threshold. The same trends are shown to occur for a square enclosure oriented vertically [7,8], which also agrees with the results of Markham and Rosenberger [9]. Effects of surface reactions, and irregular thermal profiles are considered by Zappoli [10] and Extremet et al. [11] for horizontal rectangular enclosures. Zhou and Zebib [12] show the parametric range for which flow fields bifurcate from steady to oscillatory for double diffusive flows inside horizontal enclosures in PVT. This model considers PVT inside a vertical enclosure for which the dynamical state of the flow field is beyond the critical state for a range of parameters.

The purpose of this research is to examine computationally the local and global bifurcations of flow fields in PVT for practical ground-based crystal growth conditions in order to predict their dynamical states, and to delineate growth conditions for a microgravity experiment. This will allow testing of the hypothesis that for a system far from thermodynamic equilibrium, a change in the gravitational level can shift its dynamical state. The results are compared to LDV measurements, and other experiments to correlate crystal quality with practical growth conditions. The local bifurcations show that for a fixed aspect ratio, as the Rayleigh number increases the flow bifurcates from steady to oscillatory for practical growth conditions. The steady regime consists of both diffusive-advective and diffusive-convective flows. The global bifurcation of the flow shows that in the neighborhood of the critical Rayleigh number the flow field bifurcates from uniform flow to an asymmetric cell. This corresponds to the transition from diffusive-advective to diffusive-convective flow. Subsequent global bifurcations as the Rayleigh number increases show a bifurcation to a symmetric double cell structure. Depending on the range of the Rayleigh number, the symmetric structure bifurcates to a number of asymmetric modes which leads to a traveling wave. The traveling wave either decays or persists. In the nonlinear regime, the flow switches from steady to aperiodic. Computations of asymptotic states of the flow show that these oscillations do not decay and proceed during the entire crystal growth. We show the existence of a traveling wave for this parametric range. Traveling wave state has been shown to occur in double-diffusive Rayleigh-Bénard systems, Yahata [13]. The

traveling wave state is correlated with a decrease in crystal quality [2] as measured through light scattering for the given parametric value. We show, for the condition which corresponds to the traveling wave state, that a typical microgravity environment of $10^{-3}g_0$ stabilizes the flow field and results in a diffusive-advective flow.

This paper is organized as follows. We review briefly the physics of PVT and then compare our computational results to recent LDV experiments. The dynamical state of the flow field is correlated with crystal quality for a range of practical crystal growth conditions. From the analysis of these results a critical microgravity experiment is proposed.

2. Mathematical Formulation

PVT occurs inside a vertical enclosure for source temperature T_S greater than the sink crystal temperature T_C , Figure 1. For $\Delta T > 0$, the source material A sublimates through an inert component B, and condenses at the sink. The inert component B is assumed to be rejected at the source/sink interfaces. The phase boundaries at the source and sink are at thermodynamic equilibrium, which fixes the mass fractions, ω_S and ω_C . For a system which deviates from equilibrium, $\Delta T > 0$, motion of the binary components inside the enclosure obeys the conservation of mass, energy, balance of momentum, and species continuity. Restricting the binary system to thermal convection, $M_A = M_B$, the governing equations for the average (barycentric) velocity are restricted to the Boussinesq equations as follows:

$$\nabla \cdot \vec{V}^* = 0 \quad (1)$$

$$\bar{\rho} \frac{D\vec{V}^*}{Dt^*} = -\nabla p^* + \bar{\mu} \nabla^2 \vec{V}^* + \rho \vec{g} \quad (2)$$

$$\frac{DT^*}{Dt^*} = \alpha \nabla^2 T^* \quad (3)$$

$$\frac{D\omega_A^*}{Dt^*} = \tilde{D}_{AB} \nabla^2 \omega_A^* \quad (4)$$

where

$$\rho = \bar{\rho}(1 - \beta \Delta T)$$

$$\beta = -\frac{1}{\bar{\rho}} \left. \frac{\partial \rho}{\partial T^*} \right|_{\omega_A}$$

$$\vec{g} = n g_0 \vec{j}$$

with the following initial and boundary conditions,

Initial conditions:

$$t = 0 \quad 0 < x^* < L, \quad 0 < y^* < H$$

$$T^*(x^*, y^*, 0) = T_S^* + (y^*/H) (T_C - T_S) \quad (5a)$$

$$\omega_A^*(x^*, y^*, 0) = \omega_{AS}^* + (y^*/H) (\omega_{AC} - \omega_{AS}) \quad (5b)$$

Boundary conditions:

No slip at the left and right walls,

$$t > 0 \quad \vec{V}^* \cdot \vec{n} = 0, \quad x^* = 0, \quad x^* = H, \quad \vec{V}^* \cdot \vec{y} \quad (6)$$

Prescribed temperature and fixed mass fraction at the source and crystal boundary,

$$T^*(x^*, 0, t^*) = T_S, \quad \omega_A^*(x^*, 0, t^*) = \omega_{AS}, \quad y^* = 0, \quad \vec{V}^* \cdot \vec{x} \quad (7a)$$

$$T^*(x^*, H, t^*) = T_C, \quad \omega_A^*(x^*, H, t^*) = \omega_{AC}, \quad y^* = H, \quad \vec{V}^* \cdot \vec{x} \quad (7b)$$

Insulated and impermeable boundaries at left and right walls,

$$\nabla T^* \cdot \vec{n} = 0, \quad \nabla \omega_A^* \cdot \vec{n} = 0 \quad \text{on } \Gamma \quad \text{at } x^* = 0, \quad x^* = L, \quad \vec{V}^* \cdot \vec{y} \quad (8)$$

Mass flux condition at the boundary of the source and crystal,

$$\vec{V}^* \cdot \vec{n} = - \frac{\bar{D}_{AB}}{1 - \omega_A^*(x^*, 0, t^*)} (\nabla \omega_A^* \cdot \vec{n}), \quad \text{at } y^* = 0, \quad y^* = H, \quad \vec{V}^* \cdot \vec{x} \quad (9)$$

with vanishing tangential velocity at the interface,

$$\vec{V}^* \cdot \vec{\tau} = 0 \quad \text{on } \Gamma \quad \text{at } y^* = 0, \quad y^* = H, \quad \vec{V}^* \cdot \vec{x} \quad (10)$$

In the above equations, the normal to the internal boundary is denoted by \vec{n} , $\vec{\tau}$ its tangent, and Γ its boundary. The starred (*) variables are dimensional, \bar{V} = for all, and the overbar represents average values. The mass flux condition which consists of Fickian diffusion and bulk advective flow is relative to the fixed crystal boundary. This condition was derived by Westphal and Rosenberger [14]. The motion of the source and crystal is assumed negligible, since the velocity of the bulk fluid is much greater than the crystal growth rate. We selected to use insulating boundaries to emphasize the effects of convection. Studies comparing effects of conducting versus insulating boundaries for confined fluids inside enclosures [15] show insulating boundaries are less convectively stabilizing $Ra^c_{ins.} < Ra^c_{cond.}$. Thus the critical value for insulating boundaries represents a conservative estimate.

PVT occurs at constant total pressure,

$$P_T = P_A + P_B \quad . \quad (11)$$

The partial pressure for mercurous-chloride is estimated using the correlation

$$P_A = e^{[a - b/T^*]} \quad , \quad (12)$$

with $a = 29.75$ and $b = 11767.1$ yield P_A in Pascal units [16]. Since the presence of impurity gases is inevitable, purification experiments [17] indicate the likelihood of the presence of CO. We assume $P_B = 5 \text{ torr}$ for the estimation of the thermophysical properties from the Chapman Enskog relationships [18]. The presence of the impurity component is used as a perturbation to the thermophysical properties of mercurous chloride, this allows for a more realistic estimate of the parametric values. The gas mixture is assumed to be ideal with

$$\beta = 1/\bar{T} \quad \text{and} \quad \omega_A^* = \frac{1}{1 + (P_T/P_A - 1) M_B/M_A} \quad , \quad (13)$$

using the mass and mole fraction relations.

To determine the dynamical state of the flow field requires the solution $\vec{V}(x,y,z,t;\Pi)$ as a function of the 3 space coordinates (x,y,z) , time (t) , and a vector space Π of the independent parameters. Even with the present computational capability, the solution of the entire space-time continuum (4-dimensional) is a formidable task. However, for a subset of the parameter space Π , it is possible to reduce this task and find 3-dimensional steady state solutions $\vec{V}(x,y,z;\Pi)$. This approach will yield adequate solutions for parametric values up to the Hopf bifurcation, which is a transition from the steady to periodic state. Even though this approach is desirable for many circumstances, limitations exist. Estimation of the parameter space Π indicates that the critical parameters are outside the range for which steady-state solutions exist. Alternatively the 3-dimensional solutions of $\vec{V}(x,y,t;\Pi)$ can be obtained. This is commonly referred to as 2-dimensional unsteady, even though time is a valid dimension. To study the dynamical state of the flow field, we selected to find solutions for $\vec{V}(x,y,t;\Pi)$. The advantage to this approach is that the state of flow field can be predicted for a much wider range of the parameters in Π . However, Bontoux et al. [19] has shown that the critical parameters for 3-D steady state models are less than those predicted by 2-D models. Thus the critical values for our model represent, at best, conservative estimates for the solution of the entire space-time continuum. Even with the inherent limitations of our model, it serves as a tool to study the fluid physics of PVT beyond the steady-state solutions.

2.1 Scaling

The restriction of the above equations to two spatial dimensions reduces the momentum equations to a single equation for the vorticity field, and allows for compact representation to vorticity-stream function relationship for computation. The equations are scaled using the characteristic time, and velocity (U_c) as L^2/α , and α/L respectively. Independent characteristic lengths L and H are used for the horizontal and vertical directions. The temperature and mass fraction are normalized as $T = (T^* - T_C^*)/\Delta T$, $\omega_A = (\omega_A^* - \omega_{AC}^*)/\Delta\omega$, in which ΔT and $\Delta\omega$ equal $(T_S^* - T_C^*)$ and $(\omega_{AS}^* - \omega_{AC}^*)$, respectively. Let,

$$u^* = \frac{\partial \Psi^*}{\partial y^*}, \quad v^* = -\frac{\partial \Psi^*}{\partial x^*}, \quad \zeta^* = \frac{\partial v^*}{\partial x^*} - \frac{\partial u^*}{\partial y^*}. \quad (14)$$

The above scales yield the following dimensionless equations:

$$\frac{\partial^2 \Psi}{\partial x^2} + Ar^2 \frac{\partial^2 \Psi}{\partial y^2} = -\zeta \quad (15)$$

$$\frac{1}{Pr} \frac{\partial \zeta}{\partial t} + \frac{1}{Pr} \left[u \frac{\partial \zeta}{\partial x} + Ar v \frac{\partial \zeta}{\partial y} \right] = \left[\frac{\partial^2 \zeta}{\partial x^2} + Ar^2 \frac{\partial^2 \zeta}{\partial y^2} \right] + Ra \frac{\partial T}{\partial x} \quad (16)$$

$$\frac{\partial T}{\partial t} + \left[u \frac{\partial T}{\partial x} + Ar v \frac{\partial T}{\partial y} \right] = \left[\frac{\partial^2 T}{\partial x^2} + Ar^2 \frac{\partial^2 T}{\partial y^2} \right] \quad (17)$$

$$\frac{\partial \omega_A}{\partial t} + \left[u \frac{\partial \omega_A}{\partial x} + Ar v \frac{\partial \omega_A}{\partial y} \right] = \frac{1}{Le} \left[\frac{\partial^2 \omega_A}{\partial x^2} + Ar^2 \frac{\partial^2 \omega_A}{\partial y^2} \right]. \quad (18)$$

The mass flux conditions at the boundaries become:

$$v(x,0,t) = -\frac{Ar}{Pe} \frac{1}{(Cv-1)} \frac{\partial \omega_{AS}}{\partial y}, \quad (19a)$$

$$v(x,1,t) = -\frac{Ar}{Pe} \frac{1}{Cv} \frac{\partial \omega_{AC}}{\partial y}. \quad (19b)$$

The dimensionless parameters are:

$$Ar = \frac{L}{H}, \quad Ra = \frac{\beta \Delta T \, ng_o \, L^3}{\bar{\nu} \alpha}, \quad Pe = \frac{U_0 L}{D_{AB}},$$

$$Pr = \frac{\bar{\nu}}{\alpha}, \quad Le = \frac{\alpha}{D_{AB}}, \quad Cv = \frac{(1 - \omega_{AC}^*)}{\Delta\omega}.$$

The scaling gives rise to six independent parameters. The vector space for the parameters may be expressed as

$$\Pi = \Pi (Ra, Ar, Pe, Pr, Le, Cv). \quad (20)$$

These parameters are respectively, the Rayleigh number (Ra), the aspect ratio (Ar), the Peclet (Pe), Prandtl (Pr), Lewis (Le) numbers, and the concentration parameter (Cv). Note the use of multiple length scales, L & H for the horizontal and vertical direction, result in the explicit appearance of Ar in the governing equations. In order to show the explicit dependence of the mass flux condition on the Peclet number, we used a characteristic velocity U_o which is independent of the velocity U_c due to convection. This condition occurs because the base-state flow field is independent of buoyancy induced convection. Even if $g = 0$, there always exist a base diffusive-advective flow for $\Delta T > 0$ which is dependent on the thermodynamics. This dependence has been shown [5] through the relationship of Pe on the partial pressure as

$$Pe = \ln(P_B(H)/P_B(0)) \quad . \quad (21)$$

This equation can also be expressed as a function of the mole fraction, via, $\chi_i = P_i/P_T$. Thus the value of Pe is fixed by the thermodynamics of the process.

The above equations are solved using finite difference techniques [7]. For the aspect ratio range considered, we used a 40x90 grid size. In addition a third-order Adams-Bashforth technique was used for time discretization. The choice of grid size and time step was adequate to resolve the details of the flow field.

3. Results and Discussion

3.1 Parametric Space Variation

The parametric range for which we investigated the dynamical state of the flow field is shown in Table 1. Cases 1-3 correspond to experimental conditions for the recent LDV measurements of Kim et al. [1] of the radial velocity profile at a fixed axial location. Whereas, cases 4-9 correspond to crystal growth experiments of Singh et al. [2], which correlated crystal quality with crystal growth conditions by varying the source and sink temperature. Case 10 corresponds to case 8 in a microgravity environment with a nominal gravitational acceleration of $10^{-3}g_o$. These experiments were conducted in cylindrical ampoules; we use dynamic similarity [20] for application in rectangular coordinates in which the width of our enclosure is set equal to the diameter ($L = D$) for our parametric investigation. The aspect ratio for the cases considered is on the order of .12, the Rayleigh number range from 2.08×10^2 to 9.93×10^5 .

3.2 Local Bifurcation

Our parameter space Π dictates a functional space of six parameters. However, for the parametric range of interest, most of these parameters vary over a narrow range and can be considered as passive. This reduces the parametric space to a

codimension-one bifurcation $\Pi = \Pi(Ra)$. The local bifurcation of the flow field to delineate between steady (stationary state) and oscillatory convection (periodic state) is shown in Figure 2 as a function of the Rayleigh number. In the steady convective region the flow field may be either diffusive-advective or diffusive-convective. The diffusive-advective flow is one-dimensional and is also known as the Stefan wind. It corresponds to the base flow in PVT by which global bifurcations lead to various modes as the Rayleigh number increases. If the flow field becomes unstable as the Ra increases, the first threshold of instability leads to the diffusive-convective regime, whereby a number of modes can occur. Transient oscillations can also occur in this region, however, long time asymptotic computations show that these oscillations decay. The second bifurcation connect the stationary state to the periodic state and occurs in the neighborhood of $2.59 \times 10^4 < Ra \leq 2.08 \times 10^5$. In this region the flow field oscillations do not decay. Time asymptotic computations indicate that these oscillations proceed for the entire growth of the crystal. This periodic state causes unsteady heat and mass transport which affect the homogeneity in refractive index of mercurous chloride crystals, and hence results in a degradation of crystal quality.

3.3 Global Bifurcations

For the Rayleigh number range in Figure 2 beyond the diffusive-advective region, there exists global bifurcations of the flow field which lead to various flow field plan-forms. This is illustrated for cases 1-2 in Figures 3-4, case 3 is similar to case 2. The evolution of the flow field in Figure 3, case 1 $Ra = 1.01 \times 10^4$, shows that the flow becomes unstable against the base diffusive-advective flow ($t = 0.34$). This instability leads to an asymmetric cell ($t = 0.66$) which grows until it occupies the entire cavity ($t = 1.04$). The asymmetric unicell is further bifurcated into two asymmetric cells ($t = 1.51$). The long-time asymptotic solution shows further bifurcation to an asymmetric cell which is pushed toward the crystal. This asymmetric structure is sustained for cases 2 & 3, however the flow becomes diffusive-advective for case 1.

The difference between the flow field in vertical PVT and typical Rayleigh-Bénard (RB) convection in cavities is the mass flux through the source and sink boundaries quantified by the Peclet number. In addition in RB systems the first threshold of instability is against a quiescent state in comparison to the diffusive-advective flow in our case. The mass flux through the boundaries lifts the threshold of instability, thus Figure 2 for a RB system would be shifted to the left. The similarity between the two systems is exemplified in the experiments of Olson and Rosenberger [21] to study instability of flow fields in bottom heated vertical cylinders. Their experiment showed that the first threshold of instability leads to an asymmetric roll; the number of rolls

increase with Rayleigh number. This convection planform is in agreement with our results for rectangular geometry. In contrast, the 2-D axisymmetric model of Kim et al. [22] for PVT in cylindrical geometry predict symmetric cells. This is due to the axisymmetric constraint imposed in the 2-D model. The ability of a rectangular model to predict the convective planform in cylindrical geometry underscores the importance of dynamical similarity to investigate trends.

An increase in the Rayleigh number ($Ra = 2.77 \times 10^4$) shows that the global bifurcation from diffusive-advective flow leads to symmetric cells ($t = 0.19$). This is in agreement with the experimental findings of Olson and Rosenberger [21] for the second bifurcation. The symmetry is not sustained and bifurcates to a superposed flow consisting of an asymmetric cell and uniform flow near the left wall ($t = 0.31$). The flow field is subsequently transformed from a core driven flow to a boundary layer driven flow indicated by the temperature and concentration contours ($t = 0.40$); at this point the flow field is dominated by the asymmetric cell. This asymmetric cell is subsequently bifurcated to a number of asymmetric cells ($t = 0.44$). Subsequent bifurcations $t \geq 0.52$ show the existence of an extended traveling wave. The long time asymptotic solution shows that the traveling wave decays, and the flow becomes steady with a single cell asymmetric planform. The time history of the flow field at a fixed point in the flow also shows the decay of the oscillations.

3.4 Comparison with LDV Experiments

Case 2 corresponds to the experimental condition for which the velocity profile was measured by LDV. In spite of the limitations of our model as we had pointed out, comparison with the experimental data of Kim et al. [1] show reasonable agreement, Figure 5. The magnitude of the flow is within the experimental measurements. However, the model shows a steeper velocity gradient near the wall. The asymmetry of the velocity profile is correctly predicted by our model. Case 3 shows similar agreement, however, the direction of the flow field is opposite to that predicted by the experiments. This is reminiscent of Rayleigh-Bénard cells inside a cavity for which equal probabilities exist for the sense of rotation of the cells. Case 1 also shows reasonable agreement for short time, however, long time asymptotic computation shows that the flow field gains stability. In view of the recent work by Rosenberger et al. [23], it must be pointed out that even though this 2-D unsteady model predicts reasonable trends in the core of the flow field, it may not be adequate for the prediction of crystal growth rates.

3.5 Correlation of Crystal Quality with Dynamical State of the Flow Field

To determine the effects of crystal growth experimental conditions, hence convection, on crystal quality, a number of experiments were carried out by Singh et al. [2]. The temperature difference between source and sink were varied in order to effectively vary the transport conditions which are characterized by the Rayleigh number and the remaining parameters, cases 4-9 in Table 1. The crystal quality was quantified by light scattering through the crystal, birefringence interferograms, and x-ray rocking curves. All three techniques indicated a deterioration in crystal quality with increasing Rayleigh number, cases 5,6,8. An example of the light scattering results as a function of the Rayleigh number is shown in Figure 6. The spread in the sidelobes for the largest Rayleigh number indicates an increase in inhomogeneity which causes variation in the refractive index. The inhomogeneity is attributed to the convective state during crystal growth, since all other parameters were kept fixed.

The convective characteristics as a function of the Rayleigh number, for the crystals in which the quality was quantified, is shown in Figure 7. For the lowest Rayleigh number ($Ra = 6.48 \times 10^2$), the flow is diffusive-advective and represents an optimal condition for crystal growth. As shown in Figure 6, the best quality crystal was obtained for those conditions. For increasing Rayleigh number, a sequence of bifurcations occur which results in various asymmetric modes. The global bifurcations for cases 6 & 7 are similar to cases 1 & 2, thus the time sequences are not shown. For $Ra = 1.06 \times 10^4$, the first bifurcation from the diffusive-advective flow yields an asymmetric cell which is further bifurcated to two cells as shown. In contrast, for $Ra = 2.59 \times 10^4$ the first bifurcation yields two symmetric cells, similarly to case 2 transient oscillatory convection which results in a traveling wave occurs. Asymptotic solutions show that the flow field for both cases 6 & 7 become steady and yields an asymmetric cell near the crystal. However, for $Ra \geq 2.08 \times 10^5$, the oscillations do not decay in time. The global bifurcation sequences illustrating the traveling wave state for this case are shown in Figure 8. The flow bifurcates from diffusive-advective to a symmetric mode and subsequently to multiple asymmetric cells ($t = 0.059$). As time increases an extended traveling wave propagates alternatively from source to sink $t = 0.081 \rightarrow 0.177$. Defect structures are also formed during the wave propagation. Long time asymptotic solutions show a transition from extended to localized traveling wave near the crystal interface. The traveling wave state is further illustrated in Figure 9 by the stream surface plots. Propagation of the traveling wave near the crystal and its reflection as it travels toward the source is shown. The dynamics for case 9 is similar to case 8.

4. Dynamical State of the Flow Field

The dynamical state of the flow field for the parametric range in Table 1 shows that the state of the flow field range from steady to aperiodic. In some cases the oscillations decay, in order insure that the dynamical state of the flow field is correctly predicted, we carried out asymptotic computations as pointed out by Goodrich et al. [24] for the representative cases. Large storage requirements are necessary for these cases on the order of 1 gigabyte of data. The dynamical state is predicted from the time history of the flow, phase space trajectory and power spectrum. We use the Cooley-Tukey algorithm [25] with fast fourier transforms to evaluate the power spectrum. The time step is small, such that the Nyquist frequency criterion is satisfied, thus eliminating aliasing. The power spectrum and its smoothing is calculated respectively from

$$\tilde{P}_u(f) = \left\{ \frac{1}{R} \right\} \int_0^R u(t) e^{-j2\pi ft} dt \quad (22)$$

$$P_v(f) = W_S(f) * \tilde{P}_v(f) \quad (23)$$

$W_S(f)$ is a Hanning spectral window used in the convolution relationship with the estimated power spectrum $\tilde{P}_v(f)$ to obtain the smooth spectral estimate. The time interval is denoted by R .

The dynamical state of the flow field is illustrated in Figure 10. The time history for case 5, $Ra = 3.69 \times 10^3$, which corresponds to diffusive-advective flow shows an asymptotic approach to steady state. In contrast, in the diffusive-convective region, case 7, the flow field undergoes an aperiodic transient before settling to a steady state. An example of the bifurcation from steady to an aperiodic state is shown for $Ra = 2.08 \times 10^5$, case 8. Long time asymptotic computations show that the fluctuations never decay, they proceed during the entire crystal growth event. The broadband features of the power spectrum and the unpredictability of the system illustrated by the thick limit set in phase space indicate a chaotic state. Thus, it is not surprising that lower quality crystals result for this flow state. However, conducting case 8, in a microgravity environment of $10^{-3}g_0$, case 10, shows that the flow field becomes diffusive-advective similar to case 5 in Figure 7. An alternative method to stabilize the flow field is the use of narrow aspect ratio cavities, however, a large decrease in size of the crystals may not be suitable for device applications. Thus, the parametric range for high quality crystal growth on earth is limited. In particular, stable flow fields might not exist as the aspect ratio increases. In addition, as we had pointed out, in 3-D the critical values are lower, thus the bifurcations would be shifted to the left in

Figure 2. To obtain maximum benefit from a microgravity environment, a parametric range for which the dynamical state of the flow field is aperiodic should be selected as in case 8 for a microgravity experiment. This condition would shift the dynamical state of the flow field from chaotic to steady. Thereby, the hypothesis that for a system far from thermodynamic equilibrium, a change in the gravitational level can shift its dynamical state, can be properly tested.

5. Conclusions

We examined the local and global bifurcations of the flow field in PVT for a parametric range for which experiments, to measure the velocity profile, and to quantify the effect of these parameters on crystal quality, have been performed. The physics of PVT as predicted by our model shows reasonable agreement with the velocity profile measurements. Correlation of crystal quality with the fluid dynamic state of the flow field shows that a chaotic dynamical state is correlated with lower crystal quality. In this chaotic state, a traveling wave propagates in the flow field and provides the mechanism for unsteady transport. However, a microgravity environment, with a g -level of $10^{-3}g_0$, effectively stabilizes the flow field and provides an optimal condition for high quality crystal growth. In essence, the hypothesis that for a system far from thermodynamic equilibrium, a change in the gravitational level can shift its dynamical state, has been shown theoretically. The dynamical state of the flow shifted from chaotic to steady. The results from a microgravity experiment would prove the hypothesis.

6. Acknowledgments

Computational hardware support and graphics from D. A. Thompson is acknowledged. A flight experiment to grow mercurous chloride crystals was flown on STS-77 Spacehab-04 in May 1996 through the CCDS at UAH, post-characterization of the crystals is in progress. The computations were performed using the NAS CRAY C90 at AMES Research Center.

7. Nomenclature

Ar	aspect ratio (L/H)
\bar{D}_{AB}	molecular mass diffusion coefficient
g_0	acceleration of gravity on earth ($9.8m/sec^2$)
H	cavity height
Hm	axial location of radial velocity profile measurement

\vec{j}	unit vector in vertical direction
L	cavity width
Le	Lewis number
M	molecular weight
n	ratio denoting reduction in acceleration of gravity
p	hydrodynamic pressure
P	partial pressure
P_v	power spectrum of variable v
Pe	Peclet number based on mass diffusion
Pr	Prandtl number
R	time duration of data
Ra_T	thermal Rayleigh number
t	dimensionless time
T	dimensionless temperature
T_t	characteristic time (L^2/α)
u, v	dimensionless velocity in x and y directions ($u^*/U_c, v^*/U_c$)
U_c	characteristic velocity based on convection (α/L)
U_o	characteristic velocity based on the advective-diffusive flux
x, y	dimensionless horizontal and vertical directions ($x^*/L, y^*/H$)
W_S	spectral window
\vec{v}	for all

Greek characters

Γ	boundary of cavity
Π	parameter space
α	thermal diffusivity
β	thermal expansivity
Δ	difference
χ	mole fraction
μ	dynamic viscosity
ν	kinematic viscosity
ω	mass fraction
Ψ	dimensionless stream function ($\Psi^*/U_c L$)
∇	gradient in x and y directions

ρ density
 ∇^2 Laplacian in two directions
 ζ dimensionless vorticity ($\zeta^* L/U_c$)

Subscripts

A, B, i denote components

c crystal

s source

T total

Superscripts

* dimensional quantity

- average quantity

c critical

8. References

- [1] G.T. Kim, J.T. Lin, O.C. Jones, M.E. Glicksman, W.M.B. Duval, and N.B. Singh, J. Crystal Growth 165 (1996) 429.
- [2] N.B. Singh, M. Gottlieb, R.H. Hopkins, R. Mazelsky, W.M.B. Duval, and M.E. Glicksman, Prog. Crystal Growth and Charact. 27(1993) 201.
- [3] S.J. Yosim and S.W. Mayer, J. Phys. Chem. 64 (1960) 909.
- [4] F. Rosenberger, Physico Chem. Hydrodynamics 1 (1980) 3.
- [5] D.W. Greenwell, B.L. Markham, and F. Rosenberger, J. Crystal Growth, 51 (1981) 413.
- [6] B.L. Markham, D.W. Greenwell, and F. Rosenberger, J. Crystal Growth, 51 (1981) 426.
- [7] W.M.B. Duval, J. of Chemical Vapor Deposition, 2 (1994) 188.
- [8] W.M.B. Duval, J. of Chemical Vapor Deposition, 2 (1994) 282.
- [9] B.L. Markham, and F. Rosenberger, F., 1984. J. Crystal Growth, 67 (1984) 241.
- [10] B. Zappoli, J. Crystal Growth 76 (1986) 449.
- [11] G.P. Extremet, B. Roux, P. Bontoux, F. Elie, J. Crystal Growth 82 (1987) 761.

- [12] H. Zhou and A. Zebib, *J. Crystal Growth* 135 (1994) 587.
- [13] H. Yahata, *Prog. Theor. Phys.* 85 (1991) 933.
- [14] G.H. Westphal, F. Rosenberger, *J. Crystal Growth* 43 (1978) 687.
- [15] J.R. Carruthers, in: *Preparation and Properties of Solid State Materials*, Ed. W.R. Wilcox and R.A. Lefever (Marcell Dekker, Inc., 1977) p. 1.
- [16] V. K. Neumann and E. Lichtenberg, *Z. Phys. Chem. A* 191 (1942) 284.
- [17] N.B. Singh, R. Mazelsky, W.M.B. Duval, M.E. Glicksman, *J. Crystal Growth* 106 (1990) 61.
- [18] R.C. Reid, J.M. Prausnitz and B.E. Poling, *The Properties of Gases and Liquids*, 4th Edition (McGraw Hill Book Co., 1987, p. 392, p. 581.
- [19] P. Bontoux, B. Roux, G.H. Schiroky, B.L. Markham, and F. Rosenberger, *Int. J. Heat Mass Transfer* 29 (1986) 227.
- [20] L.I. Sedov, *Similarity and Dimensional Methods in Mechanics* (Academic Press Inc. 1961) p. 1.
- [21] J.M Olson, F. Rosenberger, F., 1979. *J. Fluid Mechanics*, 92(1979) 609.
- [22] G.T. Kim, W.M.B. Duval, M.E. Glicksman, N.B. Singh, *Modelling Simul. Mater. Sci. Eng.* 3 (1995) 331.
- [23] F. Rosenberger, J. Ouazzani, I. Viohl and N. Buchan, In print *J. Crystal Growth* (1996).
- [24] J.W. Goodrich, K. Gustafson, K. Halasi, *Computer Physics Communications*, 65 (1991) 107.
- [25] J.W. Cooley, and J.W. and Tukey, *Mathematics of Computations*, 19 (1965) 297.

Table 1 - Case Studies Corresponding to Velocimetry and Light Scattering Experiments

Case	$T_s(C)$	$T_c(C)$	ΔT°	$L(cm)$	$H(cm)$	Ar	Ra	Pr	Le	Pe	Cv
1	310	290	20	2.2	17.7	.124	1.01×10^4	.899	.404	2.49	1.091
2	320	290	30	2.2	17.7	.124	2.77×10^4	.894	.364	3.03	1.051
3	310	290	20	2.3	18.0	.127	1.15×10^4	.899	.404	2.49	1.091
4	327	323	4	1.1	9.0	.122	6.48×10^2	.911	.392	1.74	1.213
5	346	338	8	1.1	9.0	.122	3.69×10^3	.910	.392	2.79	1.065
6	360	349	11	1.1	9.0	.122	1.06×10^4	.908	.392	3.42	1.034
7	373	359	14	1.1	9.0	.122	2.59×10^4	.907	.392	3.95	1.019
8	410	390	20	1.1	9.0	.122	2.08×10^5	.905	.390	5.13	1.006
9	438	409	29	1.1	9.0	.122	9.93×10^5	.902	.391	6.02	1.002
+10	410	390	20	1.1	9.0	.122	2.08×10^2	.905	.390	5.13	1.006

+ Microgravity condition $10^{-3}g_0$ corresponding to case 8

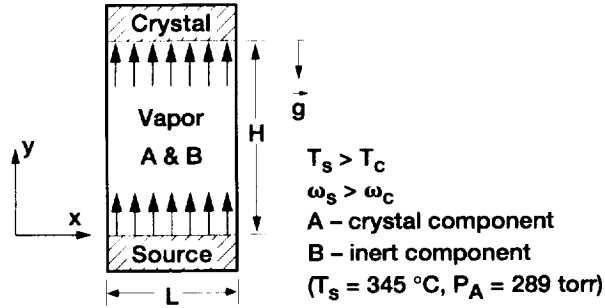


Figure 1.—Description of physical vapor transport process at typical operating conditions.

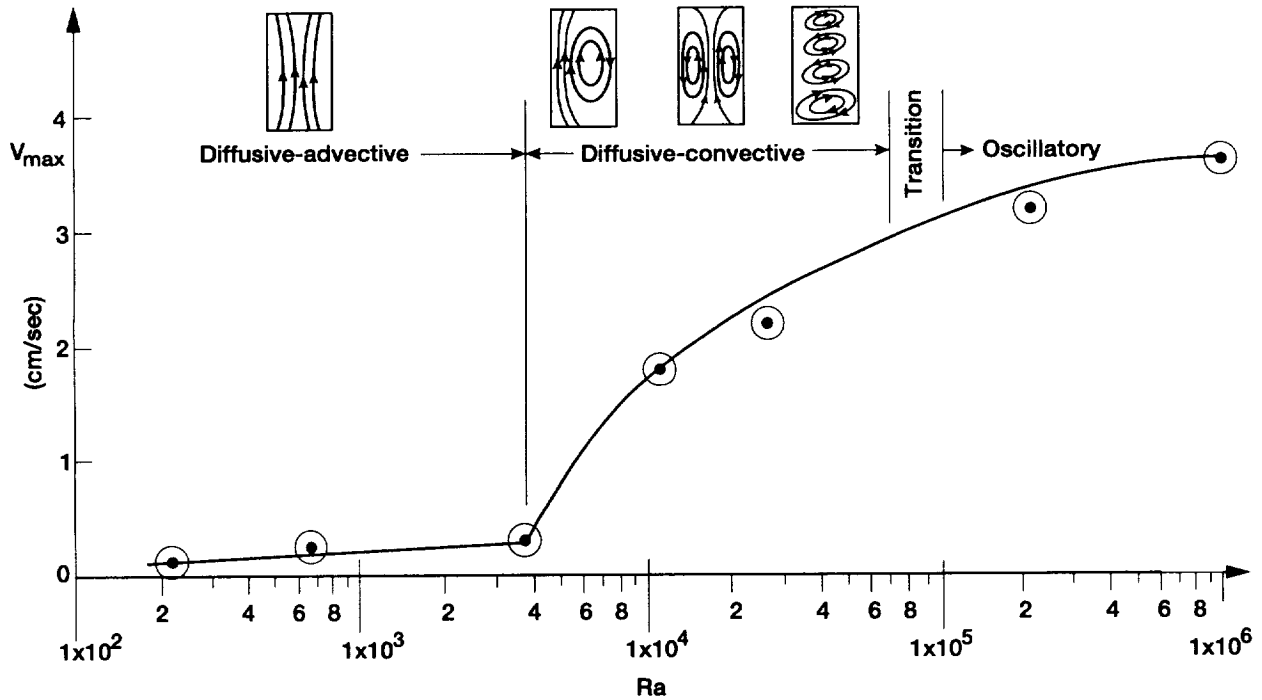


Figure 2.—Local Bifurcation diagram for $Ar = .12, 0 < Ra \leq 9.93 \times 10^5$.

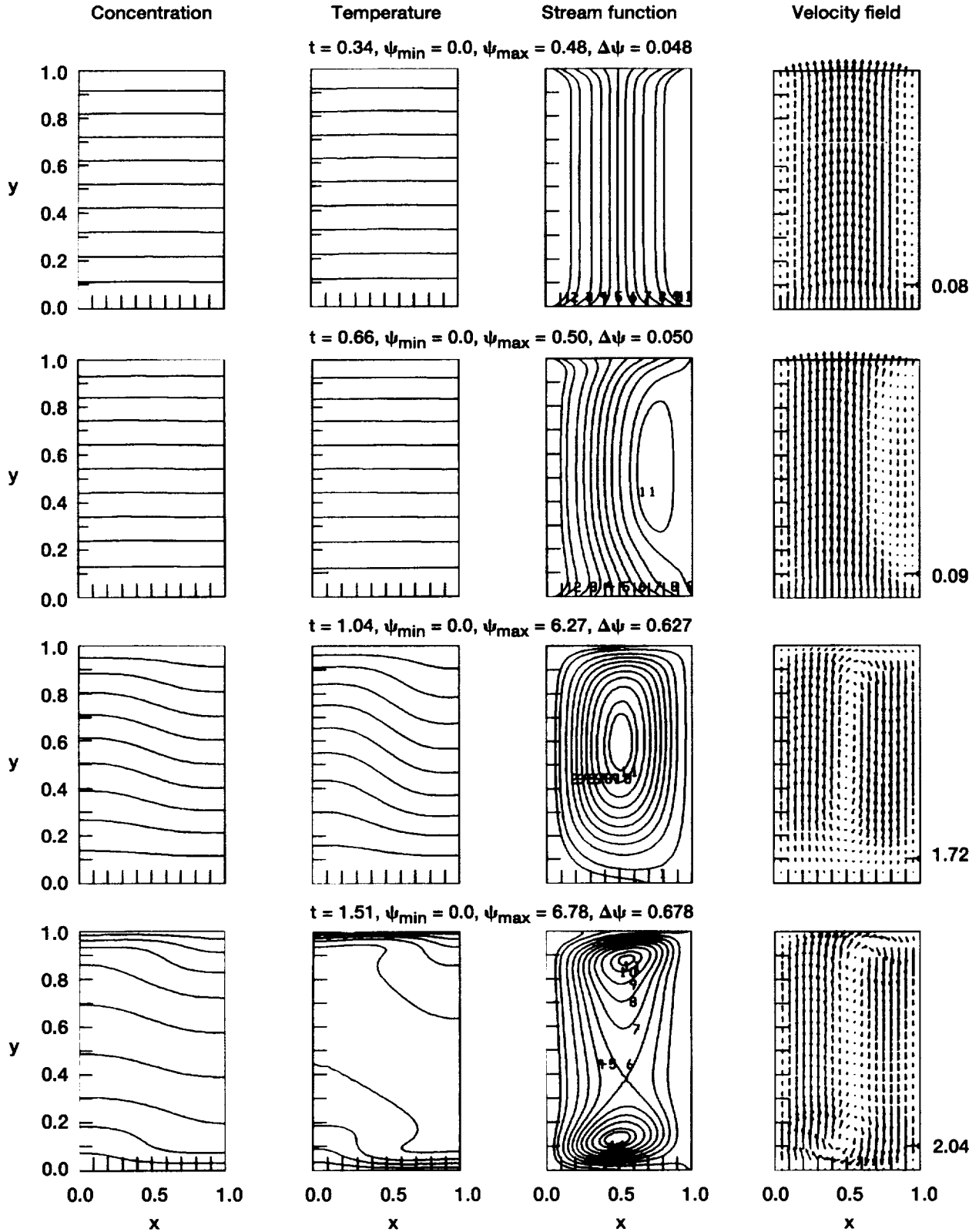


Figure 3.—Global bifurcation from diffusive-advective to asymmetric flow, $Ra = 1.01 \times 10^4$ (number at bottom of vector field plot represents maximum magnitude in cm/sec).

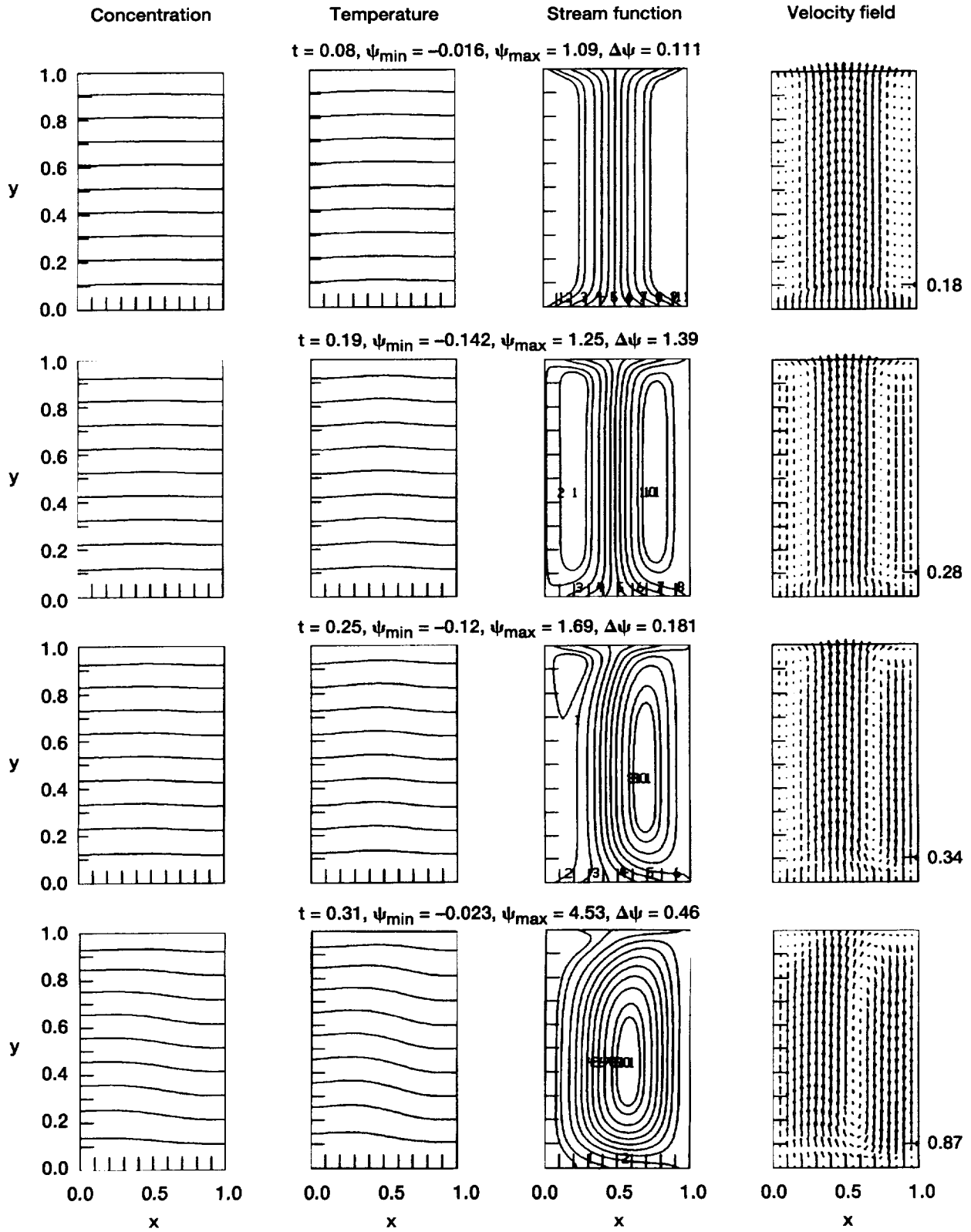


Figure 4a.—Global bifurcation from diffusive-advective to symmetric flow, $Ra = 2.77 \times 10^4$.

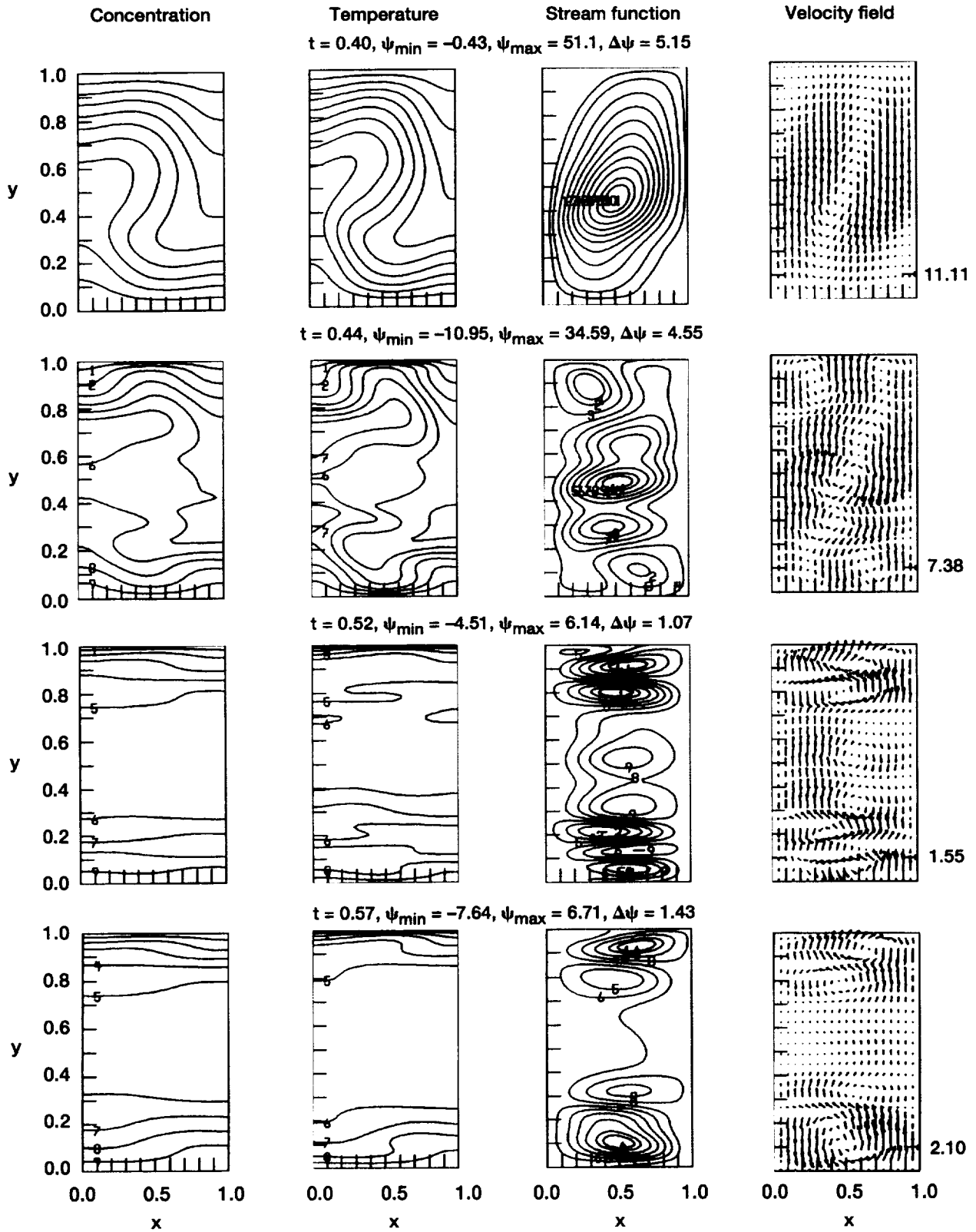


Figure 4b.—Transient traveling wave which decays in time, $Ra = 2.77 \times 10^4$.

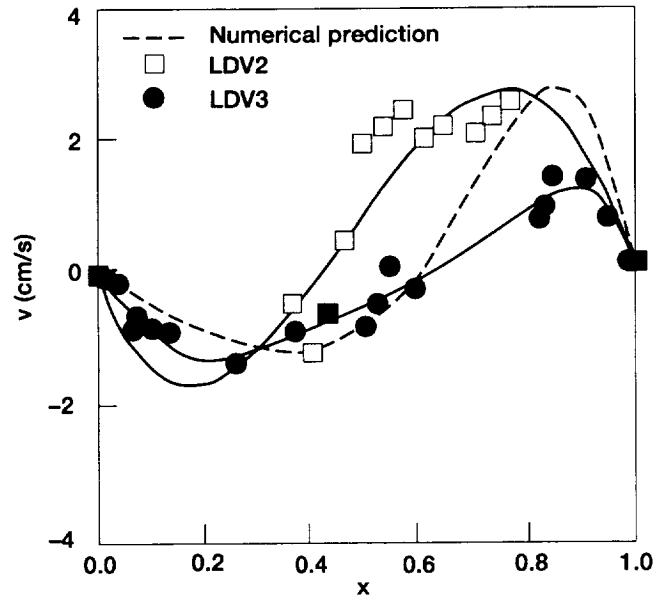


Figure 5.—Comparison of predicted velocity profile with LDV experiments of Kim et al. [1], for $Ra = 2.77 \times 10^4$ corresponding to LDV2 at location $H_m = 2.5$ cm, $t = 1.5$.

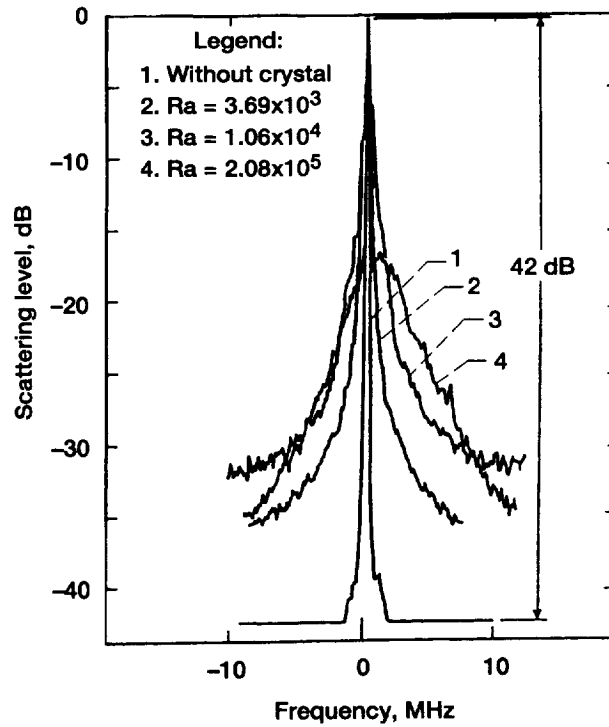


Figure 6.—Light scattering patterns through crystals as a function of Rayleigh number after Singh et al. [2].

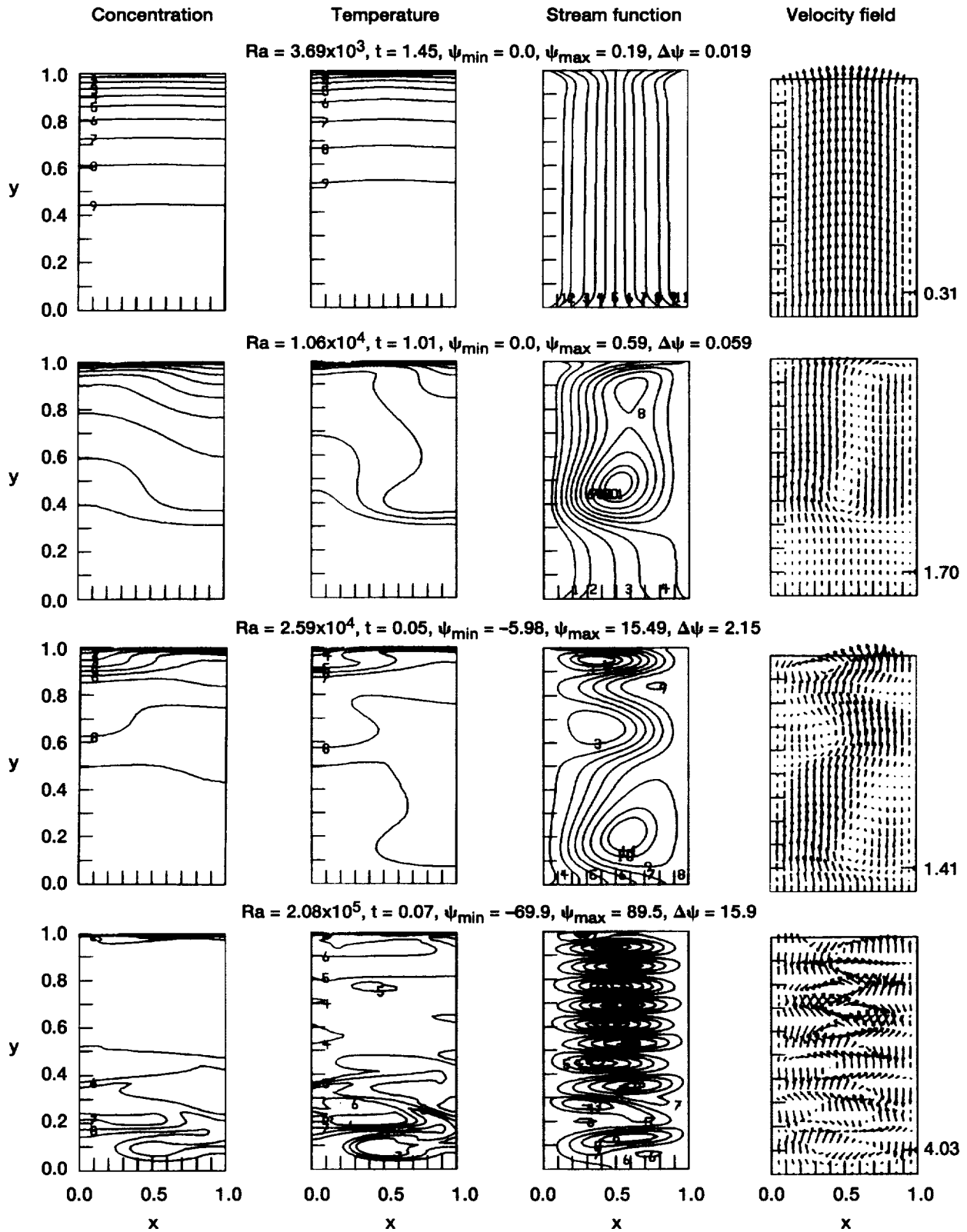


Figure 7.—Convective characteristics of flow field corresponding to light scattering patterns.

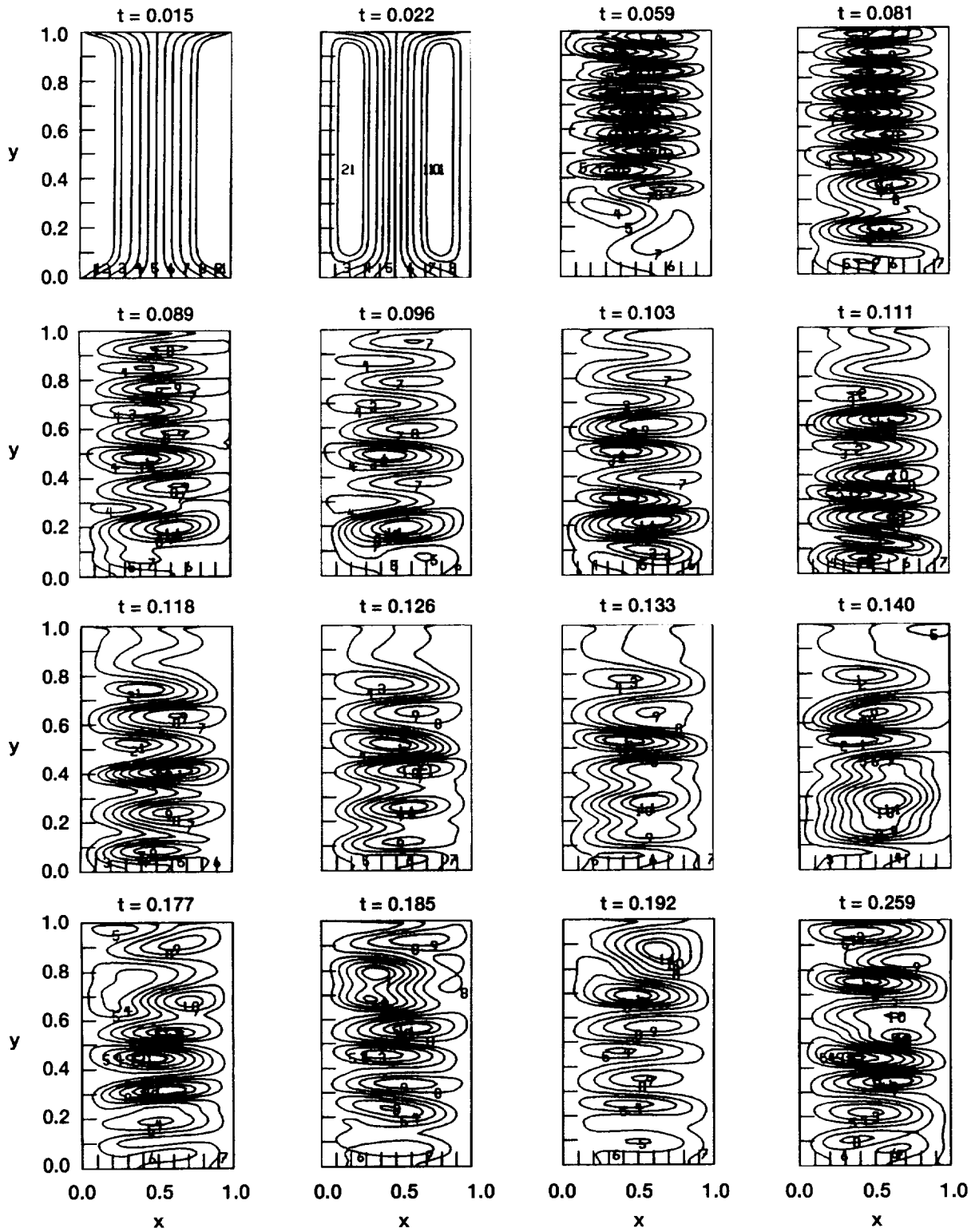


Figure 8.—Global bifurcation of flow field illustrating traveling wave state, $Ra = 2.08 \times 10^5$.

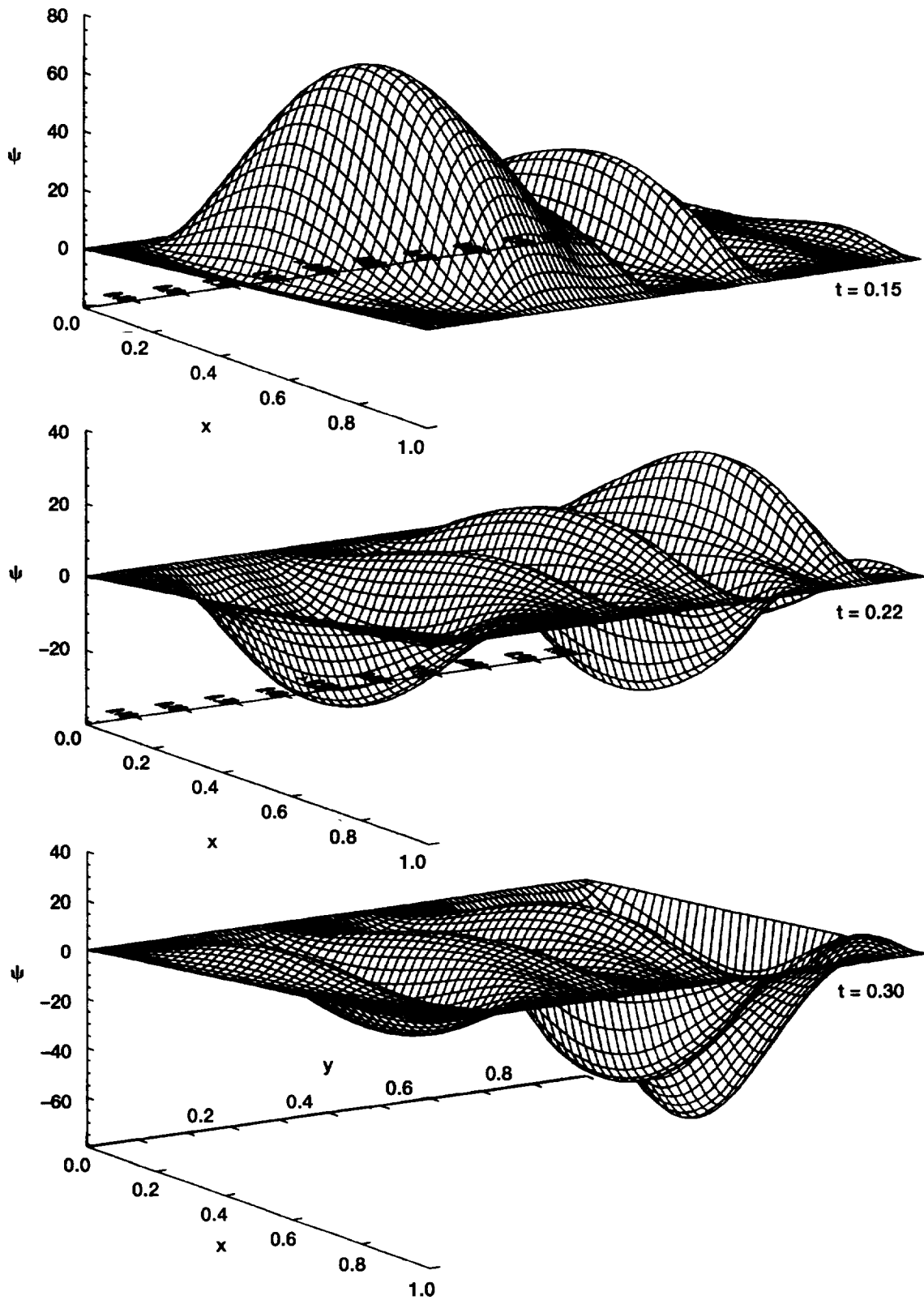


Figure 9.—Stream surface plot illustrating traveling wave, $Ra = 2.08 \times 10^5$.

REPORT DOCUMENTATION PAGE

Form Approved
OMB No. 0704-0188

Public reporting burden for this collection of information is estimated to average 1 hour per response, including the time for reviewing instructions, searching existing data sources, gathering and maintaining the data needed, and completing and reviewing the collection of information. Send comments regarding this burden estimate or any other aspect of this collection of information, including suggestions for reducing this burden, to Washington Headquarters Services, Directorate for Information Operations and Reports, 1215 Jefferson Davis Highway, Suite 1204, Arlington, VA 22202-4302, and to the Office of Management and Budget, Paperwork Reduction Project (0704-0188), Washington, DC 20503.

1. AGENCY USE ONLY (Leave blank)		2. REPORT DATE December 1996	3. REPORT TYPE AND DATES COVERED Technical Memorandum	
4. TITLE AND SUBTITLE Local and Global Bifurcations of Flow Fields During Physical Vapor Transport: Application to a Microgravity Experiment			5. FUNDING NUMBERS WU-962-20-00	
6. AUTHOR(S) W.M.B. Duval, N.B. Singh, and M.E. Glicksman				
7. PERFORMING ORGANIZATION NAME(S) AND ADDRESS(ES) National Aeronautics and Space Administration Lewis Research Center Cleveland, Ohio 44135-3191			8. PERFORMING ORGANIZATION REPORT NUMBER E-10541	
9. SPONSORING/MONITORING AGENCY NAME(S) AND ADDRESS(ES) National Aeronautics and Space Administration Washington, DC 20546-0001			10. SPONSORING/MONITORING AGENCY REPORT NUMBER NASA TM-107372	
11. SUPPLEMENTARY NOTES Prepared for the Tenth American Conference on Crystal Growth sponsored by the American Association for Crystal Growth, Vail, Colorado, August 4-9, 1996. W.M.B. Duval, NASA Lewis Research Center; N.B. Singh, Northrop Grumman Science & Technology Center, Pittsburgh, Pennsylvania 15235-5098; M.E. Glicksman, Rensselaer Polytechnic Institute, Troy, New York 12180. Responsible person, W.M.B. Duval, organization code 6714, (216) 433-5023.				
12a. DISTRIBUTION/AVAILABILITY STATEMENT Unclassified - Unlimited Subject Categories 29, 34, and 64 This publication is available from the NASA Center for AeroSpace Information, (301) 621-0390.			12b. DISTRIBUTION CODE	
13. ABSTRACT (Maximum 200 words) The local bifurcation of the flow field, during physical vapor transport for a parametric range of experimental interest, shows that its dynamical state ranges from steady to aperiodic. Comparison of computationally predicted velocity profiles with laser doppler velocimetry measurements shows reasonable agreement in both magnitude and planform. Correlation of experimentally measured crystal quality with the predicted dynamical state of the flow field shows a degradation of quality with an increase in Rayleigh number. The global bifurcation of the flow field corresponding to low crystal quality indicates the presence of a traveling wave for $Ra = 1.09 \times 10^5$. For this Rayleigh number threshold a chaotic transport state occurs. However, a microgravity environment for this case effectively stabilizes the flow to diffusive-advective and provides the setting to grow crystals with optimal quality.				
14. SUBJECT TERMS Crystal growth; Mercurous chloride; Microgravity; Convection; Dynamical stage; Bifurcation			15. NUMBER OF PAGES 27	
			16. PRICE CODE A03	
17. SECURITY CLASSIFICATION OF REPORT Unclassified	18. SECURITY CLASSIFICATION OF THIS PAGE Unclassified	19. SECURITY CLASSIFICATION OF ABSTRACT Unclassified	20. LIMITATION OF ABSTRACT	

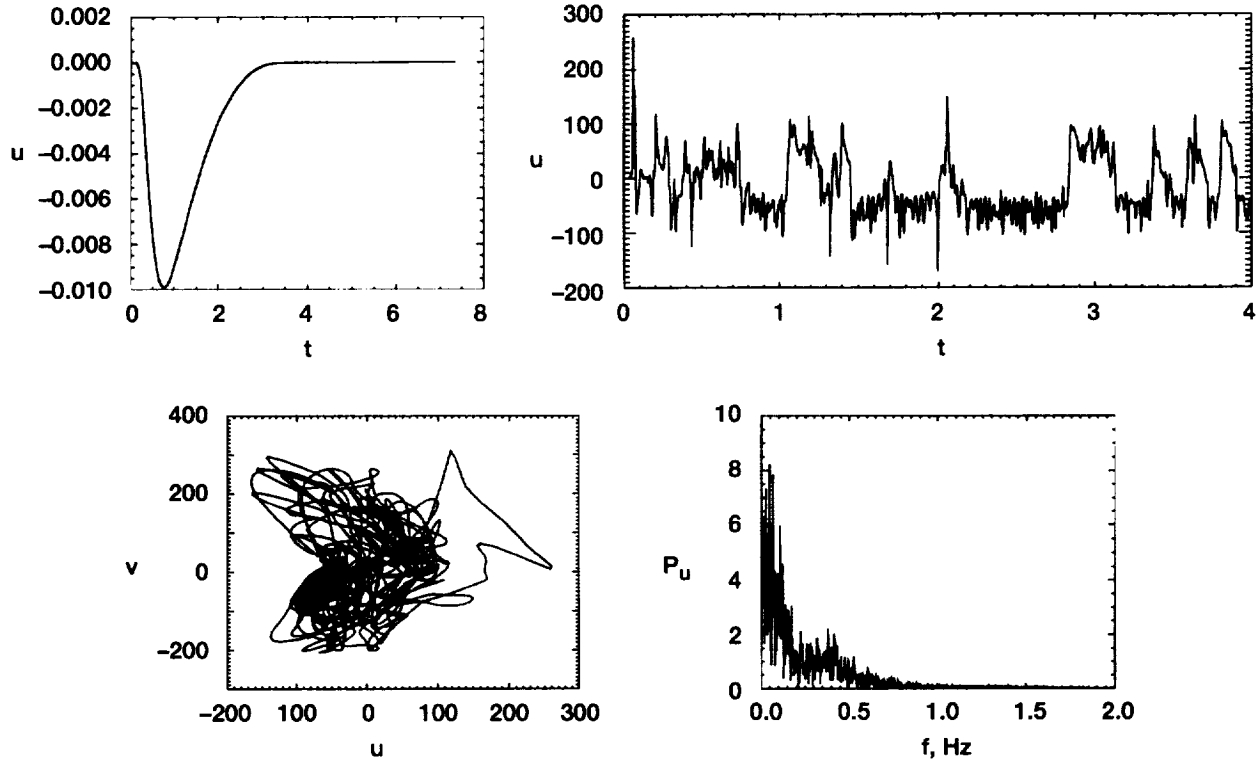


Figure 10.—Dynamical state at fixed points in flow field for cases 5, 8 (corresponding to location (0.33, 0.05), (0.05, 0.33) respectively) showing time history for cases 5, 8 $Ra = 3.69 \times 10^3$, $Ra = 2.08 \times 10^5$, and phase space trajectory and power spectrum for case 8.